Reduction in thermal conductivity and tunable heat capacity of inorganic/organic hybrid superlattices

Ashutosh Giri,[1] Janne-Petteri Niemelä,[2] Chester J. Szwejkowski,[1] Maarit Karppinen,[2] and Patrick E. Hopkins[1,*]
[1]*Department of Mechanical and Aerospace Engineering, University of Virginia, Charlottesville, Virginia 22904, USA*
[2]*Department of Chemistry, Aalto University, FI-00076 Aalto, Finland*
(Received 28 August 2015; revised manuscript received 14 December 2015; published 11 January 2016)

We study the influence of molecular monolayers on the thermal conductivities and heat capacities of hybrid inorganic/organic superlattice thin films fabricated via atomic/molecular layer deposition. We measure the cross plane thermal conductivities and volumetric heat capacities of TiO_2- and ZnO-based superlattices with periodic inclusion of hydroquinone layers via time domain thermoreflectance. In comparison to their homogeneous counterparts, the thermal conductivities in these superlattice films are considerably reduced. We attribute this reduction in the thermal conductivity mainly due to incoherent phonon boundary scattering at the inorganic/organic interface. Increasing the inorganic/organic interface density reduces the thermal conductivity and heat capacity of these films. High-temperature annealing treatment of the superlattices results in a change in the orientation of the hydroquinone molecules to a 2D graphitic layer along with a change in the overall density of the hybrid superlattice. The thermal conductivity of the hybrid superlattice increases after annealing, which we attribute to an increase in crystallinity.

DOI: 10.1103/PhysRevB.93.024201

I. INTRODUCTION

A new class of hybrid inorganic/organic materials grown via a combination of atomic layer deposition (ALD) and molecular layer deposition (MLD) have recently garnered much attention due to their ultralow thermal conductivities [1–3]. Integrated with their enhanced electrical, optical, magnetic, and mechanical properties in comparison to their conventional organic or inorganic counterparts, these novel nanomaterials make for attractive candidates for a wide array of applications in nanotechnology [4–7]. For example, stemming from the ultralow thermal conductivity, hybrid superlattice (SL) films have been shown to be ideal candidates for energy conversion technologies [2,3,8]. The low thermal conductivities in these SLs have been achieved by the inclusion of regularly spaced organic layers in-between thicker inorganic constituents, which drastically reduce phonon transport in the cross plane direction.

Although plenty of interest has been shown towards understanding thermal transport in organic-based nanocomposites [9–18], there has been limited studies focusing on heat capacity measurements of ALD/MLD grown nanomaterials. Understanding the energy storage potential (quantified by the heat capacity, C) along with thermal transport efficiency (quantified by the thermal conductivity, κ) is necessary for a complete understanding of energetic processes in hybrid materials.

We report on the thermal conductivities and heat capacities of TiO_2- and ZnO-based SLs with periodic introduction of organic layers in-between the thicker inorganic constituents. The thermal conductivities of the hybrid structures are shown to decrease with increasing number of organic layers in the SL structure, which is attributed to incoherent phonon boundary scattering at the inorganic/organic/inorganic interfaces. The inclusion of the periodic organic layers are also shown to decrease the overall heat capacities of these SLs. The effect of high-temperature annealing treatment increases the thermal conductivities and heat capacities of the TiO_2-based superlattices. This increase in the thermal conductivities is mainly attributed to enhanced crystallinity of the inorganic constituents after annealing, whereas, the increase in the heat capacities is mainly due to the increase in the density of the SLs due to the transition in orientation of the organic layers as a result of high-temperature annealing. This demonstrates the ability to control the thermal conductivities and heat capacities of hybrid SLs based on different atomic-scale structural mechanisms.

II. EXPERIMENTAL DETAILS

A. Sample fabrication and characterization

Hybrid SLs of $[(TiO_2)_m(Ti–O–C_6H_4–O–)_{k=1}]_n$ with $m =$ 40 and 4 were fabricated on MgO substrates at 210° C via the ALD/MLD technique [19] from $TiCl_4$, H_2O and hydroquinone (HQ) precursors (Picosun R-100 ALD reactor) as described in detail in our previous reports [2,20]. An illustration of a hybrid SL is shown in Fig. 1(a). Additionally, $[(ZnO)_m(Zn–O–C_6H_4–O–)_{k=1}]_n$ with $m = 9$ and 4 were also fabricated on Al_2O_3 substrates to complement our previous experiments, reported in Ref. [3]. Along with the SL films, control samples of purely ALD grown inorganic TiO_2 and ZnO films were fabricated.

Figure 1(b) shows the characteristic grazing incidence x-ray diffraction (GIXRD) patterns for the films tested in this study. The fact that the intensity of the peaks for the as-deposited TiO_2-based SLs are reduced compared to the purely ALD grown TiO_2 with anatase phase, suggests that the crystallinity in those samples is hindered due to the inclusion of the HQ layers. In contrast, for the ZnO-based SLs, inclusion of HQ layers for the $m = 9$ sample does not drastically hinder the peaks in the XRD patterns (that fit the typical ZnO hexagonal wurzite structure). Also, there is negligible change in the

*phopkins@virginia.edu

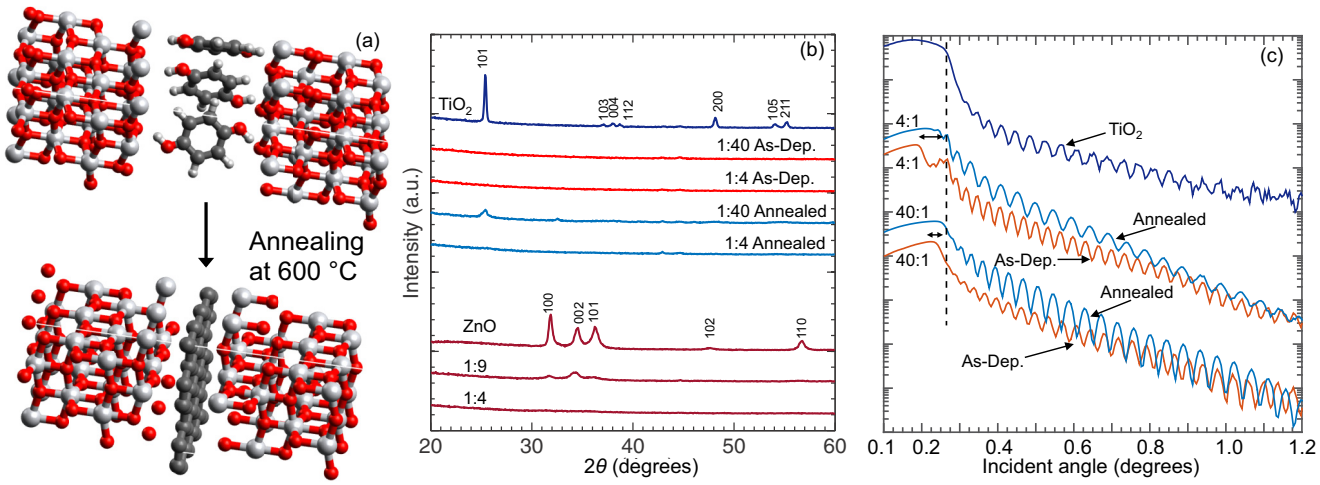

FIG. 1. (a) Schematic representation of the TiO_2-based hybrid structures for the as-deposited and annealed cases. The HQ layers transition into 2D graphitic layers due to the high annealing treatment. (b) Grazing incidence x-ray diffraction (GIXRD) patterns for the control samples and the hybrid films. (c) XRR patterns for the TiO_2 based SLs with k:m ratio of 1:40 and 1:4, as well as for the purely inorganic TiO_2 film.

position of the peaks, implying that the crystallinity for this sample is fairly conserved. The $m = 4$ samples for both ZnO and TiO_2-based SLs are amorphous in nature.

In order to enhance the crystallinity of the TiO_2-based SLs, the samples were heat-treated at 600 °C for 6 hours (Nabertherm GMbH RS 80/500/11). For the k:m = 1:40 TiO_2-based SL (with inorganic period thickness of ∼2 nm), the high annealing treatment leads to enhanced crystallinity, whereas, for the k:m = 1:4 TiO_2-based SL, GIXRD pattern does not show any change compared to the 1:4 as-deposited SL. Furthermore, the annealing process converts the molecular HQ components to a 2D graphitic layer as depicted in the schematic shown in Fig. 1(a). This conversion was confirmed *via* Raman Spectroscopy and further details on the characterization of the carbon content in the fine internal interfaces for these hybrid SLs can be found in our previous report [2]. Note, this annealing treatment does not affect the periodic layering of the SLs as demonstrated by the x-ray reflectivity (XRR; PANanalytical X'Pert Pro MPD diffractometer) patterns with interference maxima due to SL reflections as shown in Fig. 1(d) of Ref. [2] for the TiO_2-based SLs with k:m = 1:200 and 1:400. However, as the layer spacing is inversely proportional to the XRR angle θ, and because the reflected intensity decays exponentially with increasing θ, we do not observe the SL reflections for our hybrid films with very small layer spacing (k:m = 1:4 and 1:40) as shown in Fig. 1(c). In theory, these hybrid films with very small layer spacing should show SL reflections at high θ angle. Therefore, we extend the measured θ range for these samples and from the observed peaks in the XRR intensity, confirm that the SLs with k:m = 1:4 and 1:40 are in fact layered structures.

The small differences in the XRR patterns seen for the as-deposited and annealed samples reveal a reduction in the film thickness and consequent increase in the film densities. The arrows in Fig. 1(c) highlight the reduction in the film thickness after annealing that underline the shifts in the critical angle (θ_c) values. The density reduction is expected to mainly stem from the contraction of the organic layers. We estimate the densities from the critical angle values of the XRR patterns [21]. First, the mean electron density values were estimated from $\rho_e = (\theta_c^2\pi)/(\lambda^2 r_e)$, where λ is the x-ray wavelength and r_e is the classical electron radius. Then, assuming elemental compositions to follow the stoichiometry of $[(TiO_2)_m(Ti–O–C_6H_4–O–)_k]_n$ or $[(ZnO)_m(Zn–O–C_6H_4–O–)_k]_n$, the mean mass densities were obtained from $\rho_m = (\rho_e A)/(N_A Z)$, where A is the average molar mass, N_A is the Avogadro constant, and Z the average atomic number. The estimated densities along with the measured thicknesses for the thin films are shown in Table I.

B. Time-domain thermoreflectance

We measure the thermal properties of the samples with the time domain thermoreflectance (TDTR) technique. The details of the experimental procedure as well as the analysis process have been discussed in Refs. [22–24]. For this study, we modulate the pump beam at different frequencies and monitor the in-phase (V_{in}) and out-of-phase (V_{out}) signals of the reflected probe beam with a lock-in amplifier. Prior to TDTR measurements, we metallize the samples with ∼80 nm

TABLE I. Thicknesses and densities of the thin films measured via XRR.

Sample	Thickness (nm)	Density (g cm^{-3})
ALD-grown TiO_2	98.3	3.65
$[(TiO_2)_{m=40}(Ti–O–C_6H_4–O–)_{k=1}]_n$ (as-deposited)	110.8	2.87
$[(TiO_2)_{m=40}(C)_{k=1}]_n$ (annealed)	95.1	3.37
$[(TiO_2)_{m=4}(Ti–O–C_6H_4–O–)_{k=1}]_n$ (as-deposited)	123.7	1.98
$[(TiO_2)_{m=4}(C)_{k=1}]_n$ (annealed)	85.3	2.83
ALD-grown ZnO	154.0	5.4
$[(ZnO)_{m=9}(Zn–O–C_6H_4–O–)_k]_n$	93.8	3.3
$[(ZnO)_{m=4}(Zn–O–C_6H_4–O–)_k]_n$	82.7	2.4

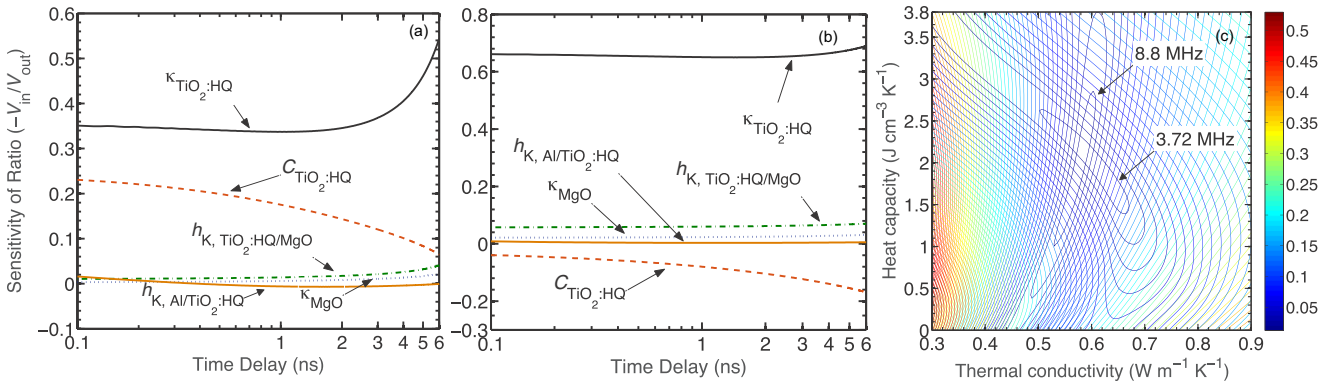

FIG. 2. Sensitivities of ratio $(-V_{in}/V_{out})$ to the thermophysical properties of the As-Dep $[(TiO_2)_{m=4}(Ti–O–C_6H_4–O–)_{k=1}]_n$ sample as a function of pump-probe time delay at (a) 8.8-MHz pump modulation frequency and (b) 3.72-MHz pump modulation frequency. (c) Sensitivity contour plot showing the interrelationship between thermal conductivity and heat capacity of the As-Dep $[(TiO_2)_{m=4}(Ti–O–C_6H_4–O–)_{k=1}]_n$ sample at 3.72-MHz and 8.8-MHz pump modulation frequencies.

of Al transducer, the thickness of which is determined via picosecond acoustics [25,26].

We analyze the TDTR data with a three-layer thermal model (layer 1: Al, layer 2: ALD/MLD SL, layer 3: semi-infinite substrate) and simultaneously measure the heat capacities and thermal conductivities of the hybrid SLs. The thermal boundary conductances at the Al/SL film and SL film/substrate interfaces have to be separated from the measurements to correctly predict the intrinsic thermophysical properties of the SL films. To this end, we analyze the sensitivity of the measurements to the various parameters in the thermal model. The sensitivity of the ratio $(-V_{in}/V_{out})$ to a thermophysical quantity is defined by [27]

$$S_x = \frac{\partial \ln(-V_{in}/V_{out})}{\partial \ln(x)}, \tag{1}$$

where x is the thermophysical parameter of interest. Figures 2(a) and 2(b) show the calculations of Eq. (1) for the sensitivity of the ratio to the various parameters in our three-layer thermal model for the TiO_2-based SL with $m = 40$ at two different pump modulation frequencies [(a) 8.8 MHz and (b) 3.72 MHz]. The most sensitive parameters are the heat capacity ($C_{TiO_2:HQ}$) and thermal conductivity ($\kappa_{TiO_2:HQ}$) of the hybrid SLs. The fact that the sensitivities are different and dynamic in nature allows us to simultaneously measure $C_{TiO_2:HQ}$ and $\kappa_{TiO_2:HQ}$ as discussed in detail below. The front side interface conductance, $h_{K,Al/TiO_2}$, and the back side interface conductance $h_{K,TiO_2/MgO}$ are measured from separate measurements on the control sample ($Al/TiO_2/MgO$). As shown in Figs. 2(a) and 2(b), the measurements are insensitive to $h_{K,Al/TiO_2}$, however, a 10% uncertainty in $h_{K,TIO_2/MgO}$ leads to a ~1.2% and ~2.4% uncertainty in $\kappa_{TiO_2:HQ}$ and $C_{TiO_2:HQ}$ at room temperature for 8.8 MHz frequency, respectively, which quantifies this insensitivity.

We confirm the measurements for $h_{K,Al/TiO_2}$ and $h_{K,TiO_2/MgO}$ by analyzing the thermoreflectance data for the control sample using two different approaches. The first approach analyzes the V_{in} as well as $-V_{in}/V_{out}$ separately, as we outline in detail elsewhere [28]. The second method utilizes two frequencies to effectively separate the interfacial conductances. At 3.72-MHz modulation frequency, we estimate an effective thermal conductivity that considers the front side conductance and the thermal conductivity of the hybrid structure as a lumped conductance. We fit the data to the model with this effective conductivity and the back side conductance as free parameters. For the higher modulation frequency (8.8 MHz), we fit the data with the free parameters as the thermal conductivity of the SL and front side conductance and assume the back side conductance as an input parameter determined from the lower modulation frequency. It should be noted that this approach to measuring the front side and back side conductances gives agreeable values to the first method outlined in Ref. [28]. Uncertainties in the measured thermal conductivities and heat capacities of the hybrid SLs are derived from the uncertainties in the input parameters and the sensitivity of the three-layer thermal model to those parameters. We measure a value of $\kappa = 5.2 \pm 0.3$ W m^{-1} K^{-1} for the purely ALD grown TiO_2 film, which is in good agreement with the literature value of ~5.7 W m^{-1} K^{-1} for an anatase thin film [29].

For a given frequency, the best fit to our TDTR signal (for hybrid SLs with high interfacial densities) can be produced with multiple combinations of the heat capacities and thermal conductivities, as shown in the sensitivity contour plots in Fig. 2(c) for a k:m = 1:4, as-deposited TiO_2-based SL. The contour plots represent the mean square deviation of the model to the TDTR data with the various combinations of C and κ as input parameters in our three-layer model [30]. Note, our best fits to the TDTR data are usually $\lesssim$0.02. As is clear from the sensitivity contour plot, a wide range of values for C can produce the best fit in the least squares sense for a given frequency. Therefore, to accurately determine C and κ, we use 3.72- and 8.8-MHz pump modulation frequencies that give different sensitivity contour maps for the thermophysical properties [see Fig. 2(c)]. The common set of values for C and κ at these two frequencies shown by the overlap of the best fit values represent our measurements for the hybrid multilayers.

III. THERMAL CONDUCTIVITY

Figure 3 shows the measured thermal conductivities for the as-deposited and annealed TiO_2-based samples with $m = 40$ as a function of temperature. Two aspects of the results shown

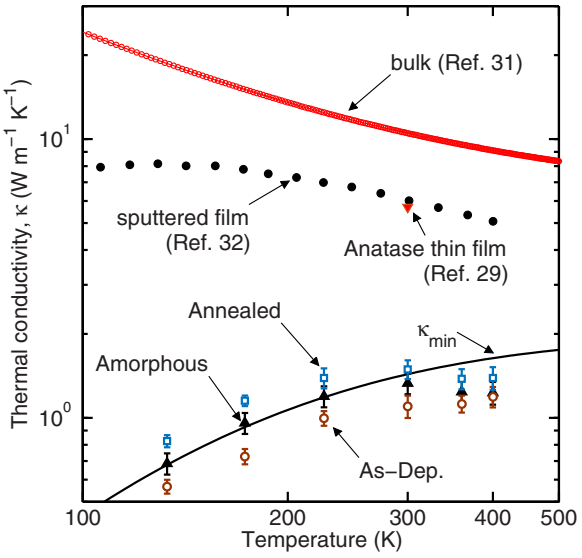

FIG. 3. Thermal conductivities of as-deposited and annealed TiO_2-based $m = 40$ SLs plotted as a function of temperature. For comparison, the measured thermal conductivities of an ALD grown amorphous TiO_2 film along with the thermal conductivities of bulk, single crystal TiO_2 (Ref. [31]), a polycrystalline sputtered film with 17-nm grain size (Ref. [32]) and anatase thin film (Ref. [29]) are also shown. The calculated minimum in thermal conductivity for TiO_2 is also shown for comparison.

in Fig. 3 are worth noting. First, the thermal conductivities measured for the as-deposited and annealed SLs show a large reduction as compared to the sputtered TiO_2 thin films [32]; at room temperature, κ for the as-deposited SL is almost 30% lower than the measured κ for an anatase thin film (Fig. 3; sold triangle) [29]. For comparison, we have also included the thermal conductivity of bulk, single crystal anatase taken from Ref. [31]. The reason for the decrease in the thermal conductivities is attributed to incoherent boundary scattering at the inorganic/organic interfaces [2]. The results for the hybrid SLs agree well with the model for the minimum limit to thermal conductivity of TiO_2 (solid black line in Fig. 3) [32,33]. For comparison, Fig. 3 also shows the measured κ for an as-deposited amorphous TiO_2 film. Even with the enhancement in crystallinity of the annealed sample, boundary scattering at the inorganic/organic/inorganic interfaces results in the low values for thermal conductivities. In Fig. 3, we have also added the predictions from a minimum thermal conductivity model for a homogeneous amorphous TiO_2 sample. This model assumes that the "mean free paths" of vibrations in the amorphous state are limited to the spacing between the atoms. Therefore, following Ref. [33], the thermal conductivity as a result from a random walk between localized oscillators is

$$\kappa_{\min} = \left(\frac{\pi}{6}\right)^{1/3} k_B n^{2/3} \sum_i v_i \left(\frac{T}{\Theta_i}\right)^2 \int_0^{\Theta_i/T} \frac{x^3 e^x}{(e^x - 1)^2} dx, \quad (2)$$

where the sum is taken over the three sound speeds (v_i), n is the atomic density, and $\Theta_i = v_i(\hbar/k_B)(6\pi^2 n)^{1/3}$ is the cutoff frequency for each polarization expressed in degrees [33]. For the calculations shown in Fig. 3 (for a homogeneous TiO_2), the longitudinal and transverse sound speeds are taken from Ref. [34]. As is clear from Fig. 3, the predicted minimum in thermal conductivity for TiO_2 agrees very well with our measured values for a homogeneous amorphous TiO_2 thin film and the thermal conductivity can be further lowered below this minimum limit by the inclusion of periodic monolayers of HQ.

The second aspect to note in Fig. 3 is the increase in the thermal conductivities of the hybrid SLs after annealing at 600 ° C for 6 hours. This can be understood as a consequence of enhanced crystallinity of the inorganic constituents due to the high annealing temperatures. However, the role of the different organic constituents (2D graphitic carbon layers in the annealed samples as compared to the HQ monolayers in the as-deposited samples) might affect the vibrational scattering mechanisms differently at these molecular interfaces. To understand the relative contributions of these two competing effects on thermal conductivity, we compare the results for the annealed and as-deposited samples with $m = 4$ as reported in our previous work [2]. We measure $\kappa = 0.62 \pm 0.04$ and 0.66 ± 0.04 W m^{-1} K^{-1} for the as-deposited and annealed samples, respectively. For these samples, even with the high annealing treatments, the inorganic constituents are mostly amorphous in nature, as demonstrated by the GIXRD patterns in Fig. 1. Consequently, the values for the measured thermal conductivities are agreeable within uncertainties, suggesting that the role of the organic layers (in these two samples with the same number of organic interfaces) in thermal transport are similar; in other words, the orientation of the HQ layer does not affect scattering at the inorganic/organic boundary and the resulting vibrational thermal conductivity. Contrary to the $m = 4$ sample, the crystallinity of the $m = 40$ sample is enhanced after annealing as demonstrated by the increase in the 101 peak [see Fig. 1(b)] and, therefore, the increase in κ is a consequence of enhanced crystallinity and not due to the intrinsic scattering mechanisms in the organic layers.

Figure 4 shows the measured thermal conductivities for the ZnO-based $m = 9$ SL as a function of temperature. Along with these measurements, we also include the measured thermal conductivities of $m = 99$ and 49 SLs from our previous work [28]. Similar to the results for the TiO_2-based SLs, the inclusion of HQ monolayers in-between the thicker inorganic constituents is shown to drastically reduce the thermal conductivities compared to the measurements of a homogeneous thin ZnO film from Ref. [35]. We have attributed the reduction in κ for the ZnO-based hybrid SLs as a phonon-boundary scattering limited process (by considering the thermal boundary conductance across ZnO/HQ/ZnO interfaces). The scattered phonon energies almost perfectly transmit across the organic monolayers (depending on the phonon wavelength), and the scattering within the organic layers itself do not contribute significantly to the overall reduction in thermal transport [28]. In comparison to the minimum thermal conductivity calculated for ZnO from the elastic constants reported in Ref. [36], κ for the $m = 9$ SL are well below the minimum limit, suggesting that the inclusion of periodic HQ layers can severely limit thermal transport in these hybrid structures.

We plot the measured thermal conductivities as a function of SL period thickness for the ZnO- and TiO_2-based SLs in Fig. 5. The results show that as the SL period thickness increases, the thermal conductivities increase monotonically for all the hybrid SLs. The drastic increase in κ as a function

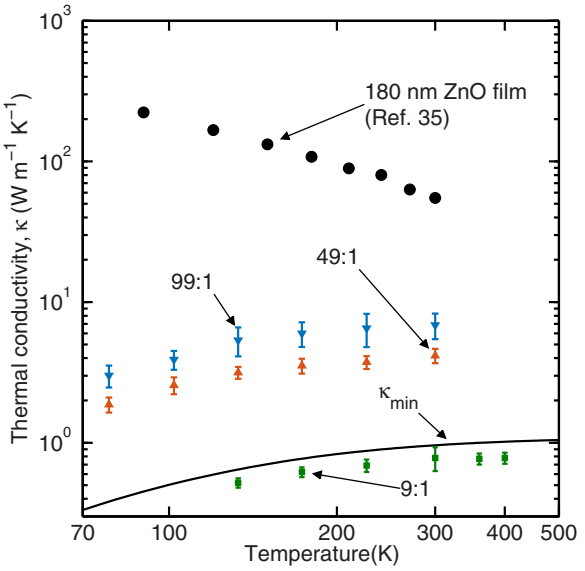

FIG. 4. Thermal conductivities of ZnO-based $m = 9$ SLs along with the thermal conductivities of $m = 99$ and 49 hybrid SLs (Ref. [28]), and a 180-nm ZnO film (Ref. [35]). The calculated minimum in thermal conductivity for ZnO is also shown for comparison.

of SL period thickness of the ZnO-based SLs as compared to the TiO_2-based SLs is due to the fact that the phonon flux in a ZnO layer is much greater than that in the TiO_2 layer [28]. Furthermore, the $m = 4$ TiO_2-based SLs and the $m = 9$ and 4 ZnO-based SLs demonstrate thermal conductivities that

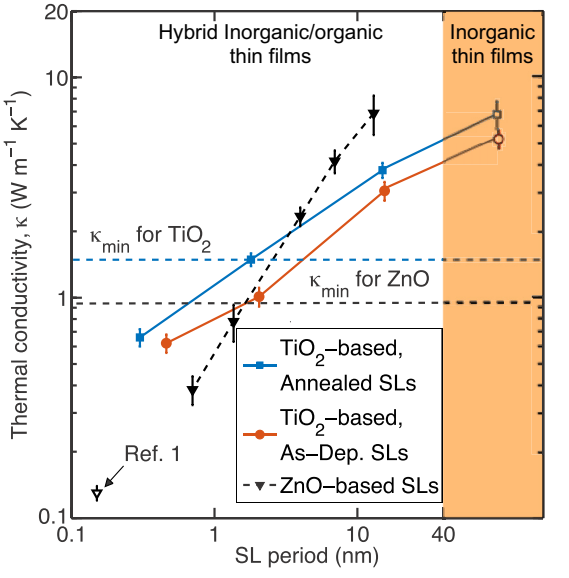

FIG. 5. Thermal conductivities of ZnO- and TiO_2-based SLs as a function of SL period thickness. The measured thermal conductivity for a k:m = 1:1 hybrid film reported in Ref. [1] is also plotted (hollow triangle). The calculated minimum in thermal conductivities for ZnO and TiO_2 are also shown for comparison. Note, for the case of as-deposited and annealed TiO_2, the SL period of $\sim$ 100 nm are for the corresponding purely ALD grown samples with $k = 0$ (hollow symbols).

are lower than the theoretical minimum, further providing evidence that the thermal transport in these SLs is severely limited by the SL period thicknesses. Figure 5 also includes the thermal conductivity measured *via* TDTR for a ZnO-based ALD/MLD grown thin film with k:m = 1:1 [1]. We estimate the period spacing for the ZnO layers in their structure to be $\sim$0.15 nm, which is a reasonable estimation considering that the average growth rate reported in Ref. [1] is 0.15 nm/cycle. Their measured thermal conductivity is in line with the decreasing trend in the thermal conductivity with decreasing period spacing for our hybrid samples. With more than an order of magnitude difference in the measured thermal conductivities, ALD/MLD grown hybrid films in general demonstrate a wide range of tunability in the design of their thermal conductivities.

IV. HEAT CAPACITY

Figure 6 shows the measured volumetric heat capacities for the TiO_2- and ZnO-based SLs as a function of temperature. Along with the thermal conductivities, the heat capacities of the TiO_2-based SLs increase significantly due to the high annealing treatment as shown in Fig. 6(a). For comparison, the bulk heat capacities of TiO_2 are also shown [38]. As expected, the heat capacities of the as-deposited SL are close to the values for the bulk heat capacities due to the fact that the fraction of the organic component in the SL film is relatively small (the SL is fabricated with 40 ALD cycles for every 1 MLD cycle). Similarly, the measured heat capacities for the ZnO-based sample (with $m = 9$) agree very well with the bulk ZnO heat capacities [Fig. 6(b)] [37].

To understand the effect of higher fractions of organic constituents on the heat capacity of the hybrid SLs, we

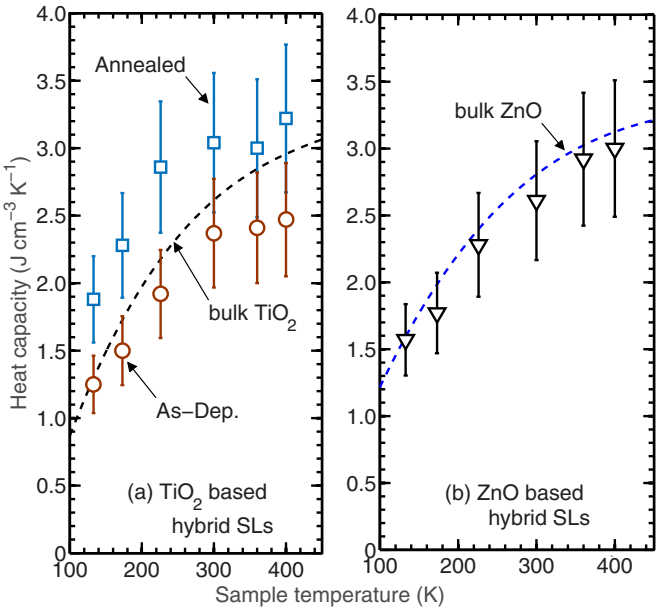

FIG. 6. Measured volumetric heat capacities as a function of temperature for (a) $[(TiO_2)_{m=40}(Ti–O–C_6H_4–O–)_{k=1}]_n$ and (b) $[(ZnO)_{m=9}(Zn–O–C_6H_4–O–)_{k=1}]_n$ SLs. The corresponding bulk heat capacities for the inorganic constituents are also shown for comparison [37,38].

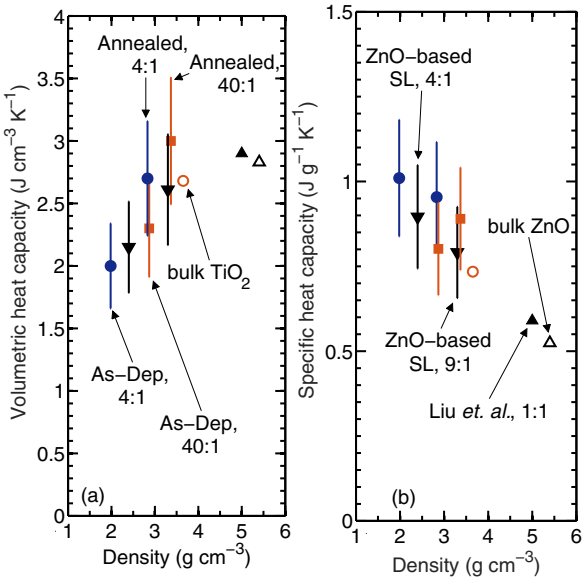

FIG. 7. (a) Volumetric heat capacities of the TiO_2- and ZnO-based thin films plotted as a function of density along with the values of bulk heat capacities for the corresponding inorganic constituents. (b) Specific heat capacities plotted as a function of density. In these plots, the data are designated as follows: TiO_2 (circles), ZnO (triangles), corresponding bulk (open symbol), ALD/MLD SLs (closed symbols). For comparison, the heat capacity measured by Liu *et. al.* [1] for a k:m = 1:1 ZnO-based hybrid film is also plotted in the figures.

compare the results for the SLs with varying number of organic monolayers as a function of their densities in Fig. 7(a). The conversion from a HQ monolayer to a 2D graphitic layer results in the decrease of the thicknesses of the annealed samples, as mentioned earlier (Fig. 1). As a result, the densities of the annealed samples increase considerably (as determined from XRR measurements of the thin films). Since the volumetric heat capacity of a substance is directly proportional to mass density, therefore, the volumetric heat capacity plotted in Fig. 7(a) increases monotonically for the as-deposited samples as the density increases. The inclusion of more HQ in the SLs decreases the volumetric heat capacity in general due to the reduction in density with higher MLD cycles. However, the volumetric heat capacities of the annealed samples (with the 2D graphitic layers) are greater than the as-deposited samples as well as that of the corresponding inorganic bulk constituent for the TiO_2 SLs, as mentioned in the previous paragraph.

Figure 7(b) shows the measured specific heat capacities of the materials calculated by dividing the measured volumetric heat capacities by their respective measured mass densities (hence, we define the specific heat capacity based on mass, where the specific heat capacity, c, is given by $c = C/\rho$, where ρ is the mass density). As is expected, the specific heat capacities of the hybrid SLs deviates from the value of the bulk inorganic constituent as the number of organic monolayer increases. At room temperature, the specific heat of the as-deposited TiO_2- and ZnO-based SLs with $m = 4$ is closer to the value of the organic counterpart, i.e., polyphenylene oxide (1.204 J g^{-1} K^{-1}). Whereas, the specific heat capacities of the SLs with $m = 40$ and 9 for the TiO_2- and ZnO-based SLs, respectively, approach the value of their corresponding inorganic constituents. Unlike the change in the volumetric heat capacities after the high annealing treatment, the specific heat of the annealed SLs show good agreement within uncertainties with their as-deposited counterparts (even though the densities increase with annealing). In Fig. 7(b), we have also included the measured specific heat of a k:m = 1:1 ZnO-based hybrid sample reported in Ref. [1] (with a density of 5 g cm^{-3}). Their result matches the decreasing trend in the measured specific heat with increasing mass density as with our hybrid multilayers.

V. SUMMARY

In summary, we have measured the thermal conductivities and heat capacities of TiO_2- and ZnO-based hybrid SLs with periodic organic layers between the inorganic constituents. The inclusion of organic layers is shown to drastically reduce the thermal conductivities of these SLs. Furthermore, the thermal conductivities of these hybrid SLs increases monotonically with increasing period thickness, suggesting that boundary scattering at the inorganic/organic/inorganic interface dominates the heat transfer in these structures. Similarly, the inclusion of organic layers are also shown to decrease the heat capacities. The effect of high-temperature annealing treatment on the TiO_2-based SLs is shown to increase both the thermal conductivities and heat capacities. The increase in thermal conductivities due to annealing is attributed to the enhanced crystallinity (not due to any intrinsic vibrational properties of the organic layer), whereas, the increase in heat capacities is attributed to the increase in the densities of the samples.

ACKNOWLEDGMENTS

P.E.H. appreciates support from the United States Army Research Office (W911NF-13-1-0378). M.K. appreciates support from the European Research Council under the European Union's Seventh Framework Programme (FP/2007-2013)/ERC Advanced Grant Agreement (No. 339478).

[1] J. Liu, B. Yoon, E. Kuhlmann, M. Tian, J. Zhu, S. M. George, Y.-C. Lee, and R. Yang, Nano Lett. **13**, 5594 (2013).
[2] J.-P. Niemelä, A. Giri, P. E. Hopkins, and M. Karppinen, J. Mater. Chem. A **3**, 11527 (2015).
[3] T. Tynell, A. Giri, J. Gaskins, P. E. Hopkins, P. Mele, K. Miyazaki, and M. Karppinen, J. Mater. Chem. A **2**, 12150 (2014).
[4] B. H. Lee, B. Yoon, V. R. Anderson, and S. M. George, J. Phys. Chem. C **116**, 3250 (2012).
[5] B. Yoon, B. Lee, and S. George, ECS Trans. **41**, 271 (2011).
[6] B. Yoon, B. H. Lee, and S. M. George, J. Phys. Chem. C **116**, 24784 (2012).
[7] T. Tynell, I. Terasaki, H. Yamauchi, and M. Karppinen, J. Mater. Chem. A **1**, 13619 (2013).

[8] J. Carrete, N. Mingo, G. Tian, H. Ögren, A. Baev, and P. N. Prasad, J. Phys. Chem. C **116**, 10881 (2012).
[9] W.-L. Ong, S. M. Rupich, D. V. Talapin, A. J. H. McGaughey, and J. A. Malen, Nat. Mater. **12**, 410 (2013).
[10] W.-L. Ong, S. Majumdar, J. A. Malen, and A. J. H. McGaughey, J. Phys. Chem. C **118**, 7288 (2014).
[11] M. D. Losego, I. P. Blitz, R. A. Vaia, D. G. Cahill, and P. V. Braun, Nano Lett. **13**, 2215 (2013).
[12] M. D. Losego, M. E. Grady, N. R. Sottos, D. G. Cahill, and P. V. Braun, Nat. Mater. **11**, 502 (2012).
[13] S. Majumdar, J. A. Sierra-Suarez, S. N. Schiffres, W.-L. Ong, I. C. Fred Higgs, A. J. H. McGaughey, and J. A. Malen, Nano Lett. **15**, 2985 (2015).
[14] J. C. Duda, P. E. Hopkins, Y. Shen, and M. C. Gupta, Phys. Rev. Lett. **110**, 015902 (2013).
[15] J. P. Feser, E. M. Chan, A. Majumdar, R. A. Segalman, and J. J. Urban, Nano Lett. **13**, 2122 (2013).
[16] Y. Jin, C. Shao, J. Kieffer, M. L. Falk, and M. Shtein, Phys. Rev. B **90**, 054306 (2014).
[17] Y. Jin, C. Shao, J. Kieffer, K. P. Pipe, and M. Shtein, J. Appl. Phys. **112**, 093503 (2012).
[18] Y. Jin, A. Yadav, K. Sun, H. Sun, K. P. Pipe, and M. Shtein, Appl. Phys. Lett. **98**, 093305 (2011).
[19] P. Sundberg and M. Karppinen, Beilstein J. Nanotechnol. **5**, 1104 (2014).
[20] J.-P. Niemelä and M. Karppinen, Dalton Trans. **44**, 591 (2015).
[21] V. Holý, U. Pietsch, and T. Baumbach, *High-Resolution X-Ray Scattering from Thin Films and Multilayers* (Springer, Berlin, Heidelberg, 1999), p. 127.
[22] D. G. Cahill, Rev. Sci. Instrum. **75**, 5119 (2004).
[23] A. J. Schmidt, X. Chen, and G. Chen, Rev. Sci. Instrum. **79**, 114902 (2008).
[24] P. E. Hopkins, J. R. Serrano, L. M. Phinney, S. P. Kearney, T. W. Grasser, and C. T. Harris, J. Heat Transfer **132**, 081302 (2010).
[25] G. Tas and H. J. Maris, Phys. Rev. B **49**, 15046 (1994).
[26] C. Thomsen, J. Strait, Z. Vardeny, H. J. Maris, J. Tauc, and J. J. Hauser, Phys. Rev. Lett. **53**, 989 (1984).
[27] R. M. Costescu, M. A. Wall, and D. G. Cahill, Phys. Rev. B **67**, 054302 (2003).
[28] A. Giri, J.-P. Niemelä, T. Tynell, J. T. Gaskins, B. F. Donovan, M. Karppinen, and P. E. Hopkins (unpublished).
[29] C. Tasaki, N. Oka, T. Yagi, N. Taketoshi, T. Baba, T. Kamiyama, S. ichi Nakamura, and Y. Shigesato, Jpn. J. Appl. Phys. **51**, 035802 (2012).
[30] J. P. Feser and D. G. Cahill, Rev. Sci. Instrum. **83**, 104901 (2012).
[31] Y. S. Touloukian, R. W. Powell, C. Y. Ho, and P. G. Klemens, *Thermophysical Properties of Matter - The TPRC Data Series. Volume 2. Thermal Conductivity-Nonmetallic Solids* (IFI/Plenum, New York, 1970).
[32] S.-M. Lee, D. G. Cahill, and T. H. Allen, Phys. Rev. B **52**, 253 (1995).
[33] D. G. Cahill, S. K. Watson, and R. O. Pohl, Phys. Rev. B **46**, 6131 (1992).
[34] Y. Ding and B. Xiao, Comp. Mater. Sci. **82**, 202 (2014).
[35] J. Alvarez-Quintana, E. Martínez, E. Pérez-Tijerina, S. A. Pérez-García, and J. Rodríguez-Viejo, J. Appl. Phys. **107**, 063713 (2010).
[36] J. Serrano, F. J. Manjón, A. H. Romero, A. Ivanov, M. Cardona, R. Lauck, A. Bosak, and M. Krisch, Phys. Rev. B **81**, 174304 (2010).
[37] O. Madelung, U. Rössler, and M. Schulz, Landolt-Börnstein - group iii condensed matter, in *II-VI and I-VII Compounds; Semimagnetic Compounds* (Springer, Berlin, Heidelberg, 1999), Vol. 41B, pp. 1–5.
[38] Z.-G. Mei, Y. Wang, S.-L. Shang, and Z.-K. Liu, Inorgan. Chem. **50**, 6996 (2011).